A mostly linear model of transition to turbulence

Jeffrey S. Baggett,[a] Tobin A. Driscoll,[b] and Lloyd N. Trefethen[c]
Cornell University, Ithaca, New York 14853

(Received 23 August 1994; accepted 15 December 1994)

A simple model in three real dimensions is proposed, illustrating a possible mechanism of transition to turbulence. The linear part of the model is stable but highly non-normal, so that certain inputs experience a great deal of growth before they eventually decay. The nonlinear terms of the model contribute no energy growth, but recycle some of the linear outputs into inputs, closing a feedback loop and allowing initially small solutions to "bootstrap" to a much larger amplitude. Although different choices of parameters in the nonlinearity lead to a variety of long-term behaviors, the bootstrapping process is essentially independent of the details of the nonlinearity and varies predictably with the Reynolds number. The bootstrapping scenario demonstrated by this model is the basis of some recent explanations for the failure of classical hydrodynamic stability analysis to predict the onset of turbulence in certain flow configurations. © *1995 American Institute of Physics.*

I. INTRODUCTION

For more than a century, it has been recognized that fluid flows in many geometries become turbulent at high Reynolds numbers, even under carefully controlled circumstances. Traditionally, this phenomenon was analyzed by considering a small perturbation of the laminar flow and looking for exponentially growing solutions. Mathematically, this consists of linearizing the Navier–Stokes equations about the laminar flow, diagonalizing the resulting operator, and looking for eigenvalues in the unstable half-plane.

While this procedure successfully predicts the onset of turbulence for some flow configurations, there are other configurations for which the transition to turbulence in experiments occurs at theoretically subcritical Reynolds numbers. Notable examples are plane Couette, plane Poiseuille, and pipe Poiseuille flows. The failure of the classical analysis has generally been attributed to the linearization about the laminar flow and has led to the development of theories that modify or eliminate that step.

Recently, however, a new explanation for the failure of classical stability analysis has gained credence.[1–6] This idea questions the diagonalization step rather than the linearization itself, because in each of the configurations just mentioned, the linearized operator is highly non-normal—its eigenmodes are far from mutually orthogonal. A consequence of the non-normality is that even when all the eigenmodes of the operator decrease monotonically with time, solutions can experience large transient growth by factors that scale with the Reynolds number. The enlarged perturbations could then potentially trigger nonlinearities leading to the transition to turbulence.

Several attempts have been made to elucidate the role of the nonlinearities within this framework.[1,6] Both Boberg and Brosa and Trefethen *et al.* propose a scenario that is schematically diagrammed in Fig. 1. A small perturbation is originally governed by the linear part of the equations, which amplifies certain structures by large factors. In contrast to a normal linear process, in the non-normal case the input and output structures are different (in plane flows, for example, they may be streamwise vortices and streaks, respectively), and the linear process alone cannot sustain the growth in the perturbation. The role of nonlinearities, then, is to transform some of the outputs back into inputs, closing the feedback loop in Fig. 1 and allowing the solution to "bootstrap" to a sustained higher amplitude.

This scenario is deliberately vague about the details of the nonlinear terms of the governing equations. If detailed information about the turbulent state itself is desired, then these details must presumably be known, but as far as the qualitative fact of transition to turbulence is concerned, the only requirement is that the nonlinearities to some degree transform outputs of the linear operator into inputs.

In this paper our aim is to lend credence to the concept of nonlinearity as a generic mixer. We propose a nonlinear system in three real dimensions adapted from the model appearing in Ref. 6. Our model has a non-normal stable linear part exhibiting transient growth characteristics analogous to those of the linearized Navier–Stokes operator for plane and pipe flows. The nonlinear part of the system has two free parameters but always contributes no energy to the system, only a mixing of the state variables. We present evidence that the bootstrapping scheme illustrated in Fig. 1 applies to this model. In particular, we show that although different parameter choices lead to quite different global system behaviors, the process of transition from small amplitude to the global regime is remarkably uniform.

In the course of writing this paper, we have become aware of a closely related work to appear by Gebhardt and Grossmann.[7] Like us, these authors are concerned with justifying the scenario of Fig. 1 for transition to turbulence. Their equations are not as simple, but more closely related to the physics, and, in particular, the role of convection in limiting instabilities is treated explicitly. Gebhardt and Grossmann do not discuss what we call bootstrapping, nor do they explore the effect of generic nonlinearities and the variety of global dynamics. On the other hand, their paper includes

[a]Department of Mathematics.
[b]Center for Applied Mathematics.
[c]Department of Computer Science.

 1070-6631/95/7(4)/833/6/$6.00

many observations not touched upon here, and we recommend it highly.

Our principal conclusions are threefold: that the notion of nonlinearity as a generic mixer may capture the essence of the process of subcritical transition to turbulence; that a bootstrapping phenomenon may be central to this process, making the threshold perturbation amplitude for transition scale with a power of the Reynolds number less than -1; and that sometimes, the global topological properties of a dynamical system may be of little relevance to the phenomena of physical interest.

II. THE MODEL

Let $u(t) \in \mathbb{R}^3$ and consider the evolution equation,

$$\frac{du}{dt} = Au + \|u\| Bu, \tag{1}$$

with the initial condition

$$u(0) = \epsilon u_0, \tag{2}$$

with $\epsilon > 0$ and $\|u_0\| = 1$. Here A and B are real 3×3 matrices, as described below. We begin with the linear part:

$$A = \begin{bmatrix} -2/R & \beta(R) & 0 \\ 0 & -2/R & \beta(R) \\ 0 & 0 & -2/R \end{bmatrix}, \tag{3}$$

with $R > 0$ and $\beta(R) = 3.86\sqrt{(R+1)/R^2}$. Here A is a highly non-normal matrix whose evolution behavior exhibits a large degree of transient growth before exponential decay sets in, due to the negative eigenvalues. The parameter R, chosen in analogy with the Reynolds number in the nondimensionalized Navier–Stokes equations, regulates the amplitude and the time scale of the transient growth. The numbers 2 and $\beta(R)$ are selected so that $\|e^{tA}\|$ achieves a maximum $\approx R$ on a time scale $\approx R$; see Fig. 2. We emphasize that the defectiveness of A (it does not have a complete set of eigenvectors) has nothing to do with dynamics we study here, since we are only concerned with the non-normality of A. It could just as easily be chosen as any sufficiently non-normal, real matrix with the spectrum in the left half-plane, and we have achieved equivalent results with a nondefective choice of A.

The matrix B is any real, skew-symmetric ($B^T = -B$) matrix normalized so that $\|B\| = 1$. This leaves two degrees of freedom for B. Since B is skew-symmetric, it is easily shown that

$$\frac{1}{2}\frac{d}{dt}\|u(t)\|^2 = u^T A u;$$

thus the nonlinear term $\|u\| Bu$ conserves energy.

The direction u_0 of the initial condition is $(0,0,1)^T$. This vector is nearly parallel to the principal right singular vectors of e^{RA} (the "optimal" defined in Ref. 2) and A^{-1} (the maximally "pseudoresonant" mode[6]). The important point is that the initial condition undergoes most of the transient growth afforded by the linearized equations, i.e., that $\|e^{tA}u_0\| \approx \|e^{tA}\|$ for $t \leq R$.

III. GLOBAL BEHAVIOR

We now summarize the dynamics the model (1)–(2) exhibits for various choices of the nonlinear coefficient matrix B. A natural starting point is to characterize the fixed points of the system. Setting the right-hand side of (1) to zero, we see that u is a fixed point if and only if $u = 0$, or

$$A^{-1}Bu = -u/\|u\|. \tag{4}$$

Thus, if v is a unit eigenvector of $A^{-1}B$ with negative real eigenvalue $-\lambda$, then $u = \pm v/\lambda$ are fixed points of the system; moreover, all fixed points besides the origin correspond to such eigenpairs. Since B has rank 2, one eigenvalue of $A^{-1}B$ is zero, so the system may have 0, 1, or 2 symmetric pairs of fixed points, in addition to the origin. The Jacobian of the system (away from the origin) is

$$J(u) = A + \|u\| B + Buu^T/\|u\|, \tag{5}$$

and the stability properties of the fixed points are easy to compute. Note that $J(u) = J(-u)$, so symmetric pairs of fixed points have identical stability characteristics. Finally, the Jacobian at the origin is just A, so the origin is always a stable fixed point.

Rather than attempting to catalog the model's behavior for all possible choices of B and R, we now investigate the global dynamics for four specific choices of B_j and $R = 100$. The matrices B_j, along with their associated fixed points and eigenvalues of the Jacobian, are listed in the Appendix. These four examples are fairly typical of most of the behaviors observed over all choices of B.

The first example, B_1, produces a pair of saddle points near the origin and a pair of sinks at a distance of order 1. In this case, trajectories that escape the vicinity of the origin spiral in to one of the other two sinks, as illustrated in Fig. 3.

With $B = B_2$, the only fixed points are a pair of saddle points at a distance of order 10^{-4} from the origin. Here, solutions that leave the origin are destined to corkscrew away to infinity along one of two diametrically opposite directions, as in Fig. 4.

The third example, B_3, like the first, has two pairs of fixed points other than the origin: one pair near the origin and the other a distance of order of magnitude 1 away. In this case, however, all the fixed points are saddle points. There are now two possible global behaviors for solutions that do not decay to the origin. If the solution initially has a norm of about unity or less, the trajectory approaches one of two limit cycles, as in Fig. 5. On the other hand, if the initial condition has a norm much larger than unity, the solution spirals out slowly to infinity.

Example B_4 has a fixed-point structure qualitatively similar to that of B_3. The quantitative details, however, are sufficiently different to change the limit cycle behavior into chaos, as is shown in Fig. 6. Initial conditions of norm larger than unity still induce a spiral outward to infinity.

The behaviors described above change if R is varied. At small R (less than ≈ 20), all four examples have a pair of saddle points near the origin and a pair of sinks farther away; the dynamics resemble those depicted in Fig. 3. As R increases, the fixed points near the origin are essentially unchanged, while the other pair moves or changes type. For B_1

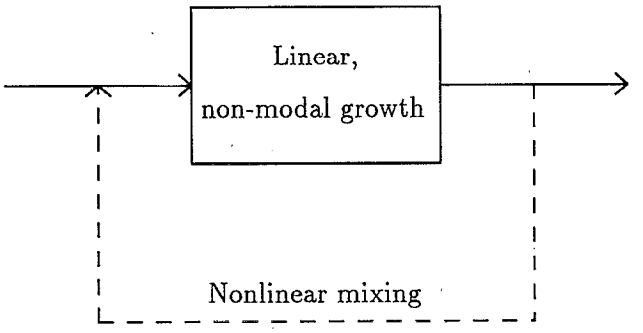

FIG. 1. "Bootstrapping" model of the transition to turbulence.

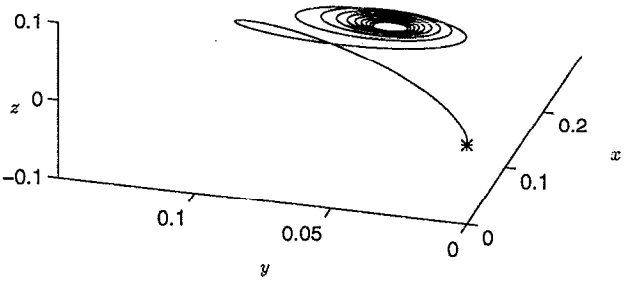

FIG. 3. Sink. [Model (1)–(2) with $B=B_1$, $\epsilon=10^{-5}$.] The origin is marked by a star.

and B_2, this pair remains stable but moves toward the origin or infinity, respectively. For B_3 and B_4, the sinks bifurcate into saddle points.

Clearly these four choices of the coefficients of the nonlinearity in (1) lead to entirely different global behaviors. We shall now show, however, that the process of a solution's transition from small amplitude into global dynamics is remarkably similar for these four cases, and indeed many others.

IV. TRANSIENT BEHAVIOR AND BOOTSTRAPPING

Consider now Fig. 7, a different presentation of the solutions for the examples presented in the last section. Here we plot, for each choice of B_j, the norm of the solution state vector as a function of time for three solutions of (1)–(2), with $\epsilon=10^{-5}$, 10^{-6}, and 10^{-7}. The curves with $\epsilon=10^{-6}$ and 10^{-7} show that these solutions grow by a factor of about R before eventually decaying exponentially, indicating that the linear part of the model dominates the dynamics for all time—in other words, the perturbation represented by the initial condition is practically infinitesimal.

The curves with $\epsilon=10^{-5}$ correspond to the solutions pictured in Figs. 3–6. These are all solutions that exhibit transition to global dynamics, and the curves for large times reflect the differences observed in the last section. Yet the initial phase looks quite similar in all four cases. Again there is a short period of growth by a factor R induced by the linear terms. Now, though, the solution has evidently become large enough to enable the nonlinear terms to close the loop diagrammed in Fig. 1. Thus, the solution begins to bootstrap its way to a much larger amplitude. As the solution grows in amplitude, the details of the nonlinearity begin to exert a noticeable influence on the solution and the system has reached a fully "turbulent" state.

Evidently, for each particular choice of B and R there is a threshold amplitude for the initial condition, above which the solution undergoes transition and below which it decays. A heuristic argument appearing in Ref. 6 predicts a simple dependence of this threshold on R. A solution starting with amplitude ϵ grows to size of order ϵR after a time of order R, as the linear nonmodal amplification transforms input structures (right singular vectors) into output structures (left singular vectors). Over the same time, the nonlinear terms return energy from outputs to inputs. This mixing is quadratic in the solution amplitude and acts over time R, so the regenerated inputs have size $R(\epsilon R)^2$. If the process is to be self-sustaining, the regenerated amplitude must be at least as large as the original: $\epsilon=O[R(\epsilon R)^2]$, yielding a threshold of $\epsilon=O(R^{-3})$. This is in contrast to one's natural first expectation that linear growth of $O(R)$ would produce a threshold of $O(R^{-1})$.

Numerically, the transition threshold can be determined for each choice of B and R by a simple bisection. In Fig. 8

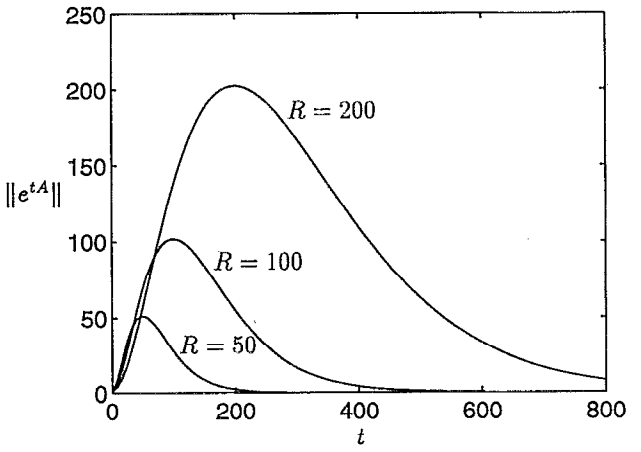

FIG. 2. Transient growth in the linearized model.

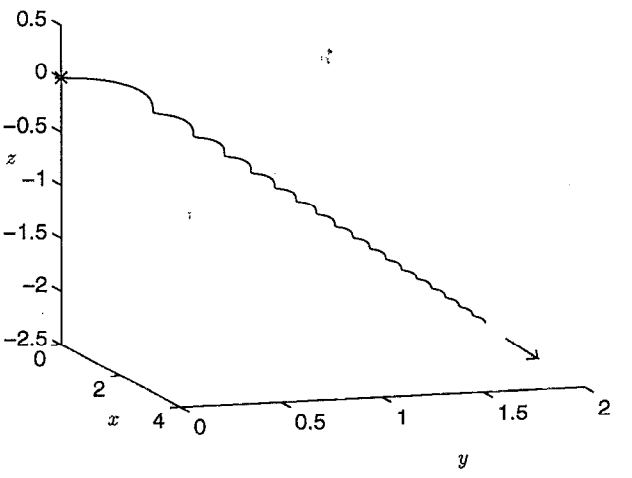

FIG. 4. Escape to infinity. [Model (1)–(2) with $B=B_2$, $\epsilon=10^{-5}$.]

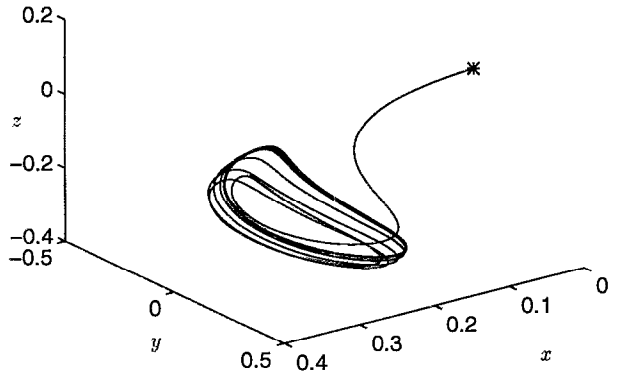

FIG. 5. Limit cycle. [Model (1)–(2) with $B=B_3$, $\epsilon=10^{-5}$.]

we show the dependence of the transition threshold on R for the four examples of Sec. III. All four examples agree excellently with the heuristic, even though the global system behavior changes for the different B_j and as R varies. Furthermore, there is nothing special about these examples. Figure 9 shows the results of the same threshold calculations for 50 random matrices B, each generated by forming a matrix with independent entries drawn from a normal distribution of mean zero, taking the skew-symmetric part, and normalizing. Asymptotically the dependence of the threshold on R is cubic, as is illustrated in the histogram of Fig. 10. In one case, no transition was observed for very low values of R, but for R greater than about 20 the threshold is finite and demonstrates cubic dependence on R.

The variation in heights of the curves in Fig. 9 is related to the efficiency of each B in transforming the principal output of the linear amplification back into the principal input. To quantify this efficiency, let u_1 and v_1 be the principal left and right singular vectors of e^{RA}, corresponding to those output and input vectors, respectively, and define the "mixing index,"

$$\gamma(B)=v_1^T B u_1. \tag{6}$$

In Fig. 11 we plot the transition threshold versus the mixing index for the 50 examples from Fig. 9, at $R=100$. When $\gamma>0$, the threshold varies as γ^{-1}, confirming that B's principal action is to transform u_1 into v_1. When $\gamma<0$, the rela-

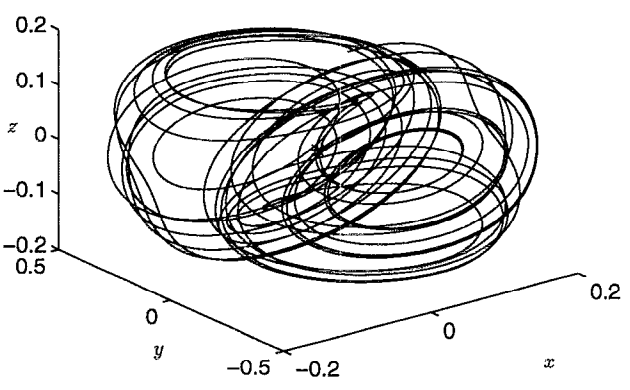

FIG. 6. Chaos. [Model (1)–(2) with $B=B_4$, $\epsilon=10^{-5}$.] The time interval $0\leq t\leq 700$ is shown.

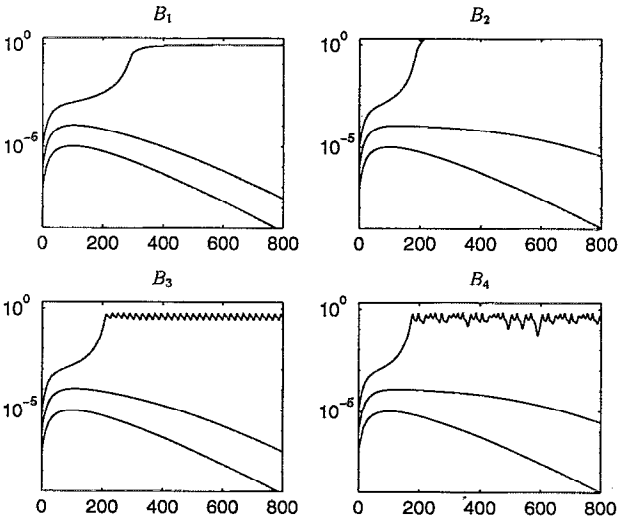

FIG. 7. Amplitude $\|u(t)\|$ vs t for model (1)–(2), with $B=B_1, B_2, B_3, B_4$, and $\epsilon=10^{-5}, 10^{-6}, 10^{-7}$.

tionship is less obvious; however, the negative feedback clearly weakens the bootstrapping mechanism. We also observe that when $|\gamma|<0.2$, there is a greater tendency than otherwise for the transition threshold to vary from cubic dependence on $1/R$. This may be because linear amplification of secondary inputs plays a more important part.

V. CONCLUSIONS

We have shown that a simple three-dimensional model (1) with linear, nonmodal amplification and nonlinear mixing demonstrates a bootstrapping phenomenon in transition from small- to large-amplitude dynamics. The non-normality of the linearized system is the only source of energy growth for solutions, and the function of the nonlinearity is just to ensure that some fraction of the linear outputs is recycled to inputs. As a result, nonlinearities that are quite different in the sense of long-term behavior are similar when it comes to transition. This has been substantiated by verifying that the

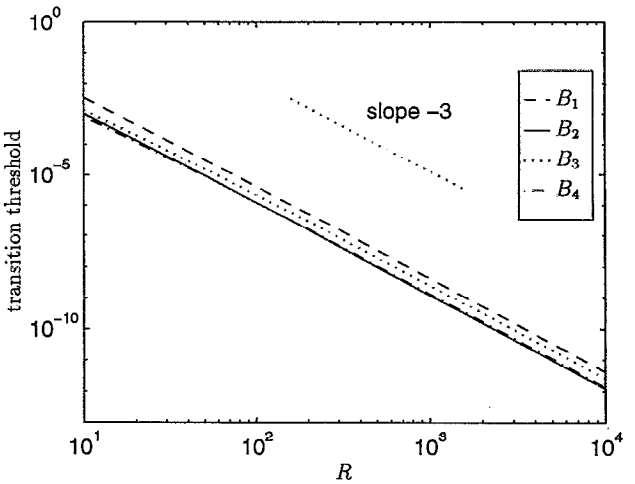

FIG. 8. Threshold amplitude for the examples in Sec. III as a function of R.

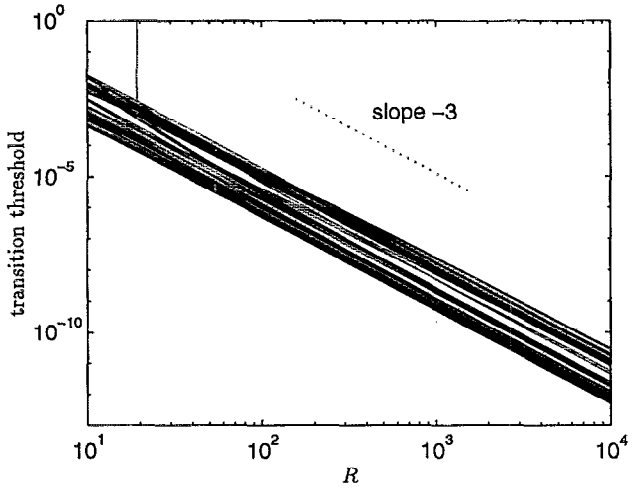

FIG. 9. Threshold amplitude for 50 random choices of B as a function of R.

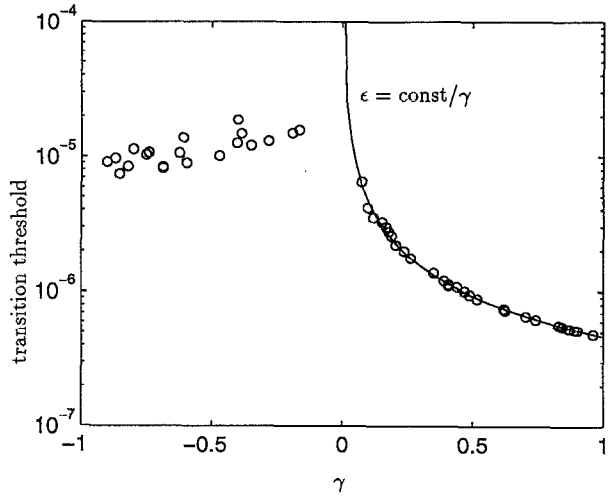

FIG. 11. Threshold amplitude versus mixing index γ at $R=100$.

transition threshold amplitude varies as $O(R^{-3})$ for random choices of coefficients in the nonlinear part of our model, in accordance with the bootstrapping heuristic.

Analogously, we believe that a transition threshold $O(R^{\alpha})$ with $\alpha<1$ is characteristic of actual plane Couette and pipe Poiseuille flows, as conjectured in Ref. 6. We do not claim that this exponent is -3. In fact, several recent works have aimed at determining how the threshold amplitude scales with the Reynolds number. Kreiss *et al.*[8] have proved, for plane Couette flow, a lower bound of $O(R^{-21/4})$ below which all disturbances eventually decay. Direct numerical simulations have revealed disturbances whose amplitudes scale as $R^{-5/4}$ and $R^{-7/4}$ for plane Couette and Poiseuille flows, respectively.[9] As mentioned in Ref. 6, the presumed reason why real flows may not exhibit an exponent as low as -3 is that the nonlinear interactions in the Navier–Stokes equations act across modes via selection rules that our simplified equations do not model.

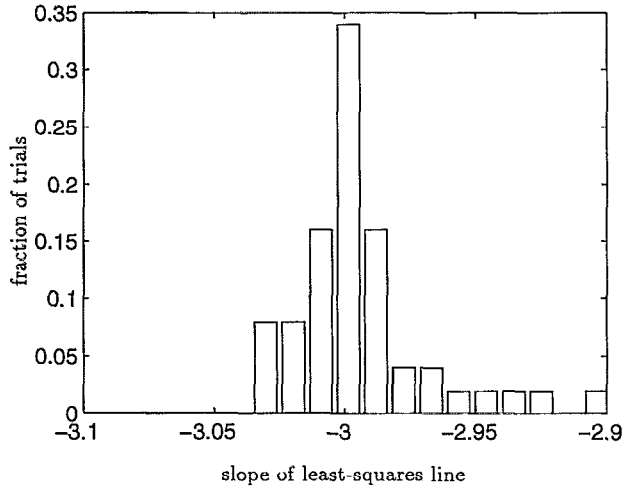

FIG. 10. Histogram of slopes in Fig. 6. Each slope is obtained from a least-squares linear fit to the threshold data for $10^3 \leq R \leq 10^4$.

Our study supports the hypothesis that nonlinearities can be viewed to some degree as generic energy mixers. Our low-order model displays a variety of global behaviors, but we do not claim that it can approach the complexity of fully developed turbulence, which is thought to be an inherently high-dimensional phenomenon. Nor do we claim that it captures the process of transition to turbulence in a physically detailed way. For example, we do not take into account the mean flow deviation, and one consequence of this is that the evolution of our disturbance does not exhibit an initial overshoot before settling to a level that is roughly independent of the Reynolds number, as is often the case in real fluid flows. In fact, our solutions can grow unboundedly. Nevertheless, we feel our model demonstrates an essential mechanism of transition to turbulence for flows with highly non-normal linearizations. The same conclusion has been reached by Gebhardt and Grossmann[7] on the basis of their more physical set of equations.

TABLE I. Fixed points of the four examples.

	First pair, spectrum of J		Second pair, spectrum of J	
B_1	$\pm\begin{bmatrix}-0.00\,047\\-2.5e{-}05\\-8.7e{-}07\end{bmatrix}$,	$\begin{bmatrix}0.0055\\-0.033\pm0.019i\end{bmatrix}$	$\pm\begin{bmatrix}-0.78\\-0.14\\0.46\end{bmatrix}$,	$\begin{bmatrix}-0.019\\-0.021\pm0.91i\end{bmatrix}$
B_2	$\pm\begin{bmatrix}-0.000\,14\\-7.0e{-}06\\-3.4e{-}07\end{bmatrix}$,	$\begin{bmatrix}0.0053\\-0.033\pm0.021i\end{bmatrix}$	...	
B_3	$\pm\begin{bmatrix}-0.000\,25\\-1.3e{-}05\\-5.3e{-}07\end{bmatrix}$,	$\begin{bmatrix}0.0056\\-0.033\pm0.019i\end{bmatrix}$	$\pm\begin{bmatrix}-0.38\\-0.22\\0.31\end{bmatrix}$,	$\begin{bmatrix}-0.086\\0.013\pm0.44i\end{bmatrix}$
B_4	$\pm\begin{bmatrix}-0.000\,14\\-7.2e{-}06\\-3.3e{-}07\end{bmatrix}$,	$\begin{bmatrix}0.0054\\-0.033\pm0.02i\end{bmatrix}$	$\pm\begin{bmatrix}-0.26\\-0.4\\0.22\end{bmatrix}$,	$\begin{bmatrix}-0.13\\0.034\pm0.48i\end{bmatrix}$

ACKNOWLEDGMENTS

This work was supported by U.S. Department of Energy Grant No. DE-FG02-94ER25199, National Science Foundation (NSF) Grant No. DMS-9116110, and an NSF Graduate Research Fellowship. We also thank Martin Gutknecht and the Interdisciplinary Project Center for Supercomputing at the Swiss Federal Institute of Technology in Zurich.

APPENDIX: MATRICES USED FOR EXAMPLES

The four matrices B_j used for the examples in Secs. III and IV are

$$B_1=\begin{bmatrix} 0 & -0.6845\ 47 & -0.114\ 036 \\ 0.684\ 547 & 0 & 0.719\ 994 \\ 0.114\ 036 & -0.719\ 994 & 0 \end{bmatrix},$$

$$B_2=\begin{bmatrix} 0 & -0.559\ 04 & -0.398\ 39 \\ 0.559\ 04 & 0 & 0.727\ 159 \\ 0.398\ 39 & -0.727\ 159 & 0 \end{bmatrix},$$

$$B_3=\begin{bmatrix} 0 & -0.910\ 217 & -0.181\ 441 \\ 0.910\ 217 & 0 & 0.372\ 269 \\ 0.181\ 441 & -0.372\ 269 & 0 \end{bmatrix},$$

$$B_4=\begin{bmatrix} 0 & -0.905\ 766 & -0.345\ 222 \\ 0.905\ 766 & 0 & 0.245\ 783 \\ 0.345\ 222 & -0.245\ 783 & 0 \end{bmatrix}.$$

The fixed points and corresponding Jacobian eigenvalues are tabulated in Table I.

[1] L. Boberg and U. Brosa, "Onset of turbulence in a pipe," Z. Naturforschung Teil **43a**, 697 (1988).
[2] K. M. Butler and B. F. Farrell, "Three-dimensional optimal perturbations in viscous shear flow," Phys. Fluids A **4**, 1637 (1992).
[3] B. F. Farrell and P. J. Ioannou, "Stochastic forcing of the linearized Navier–Stokes equations," Phys. Fluids A **5**, 2600 (1993).
[4] L. H. Gustavsson, "Energy growth of three-dimensional disturbances in plane Poiseuille flow," J. Fluid Mech. **224**, 241 (1991).
[5] S. C. Reddy and D. S. Henningson, "Energy growth in viscous channel flows," J. Fluid Mech. **252**, 209 (1993).
[6] L. N. Trefethen, A. Trefethen, S. C. Reddy, and T. A. Driscoll, "Hydrodynamic stability without eigenvalues," Science **261**, 578 (1993).
[7] T. Gebhardt and S. Grossmann, "Chaos transition despite linear stability," Phys. Rev. E **50**, 3705 (1994).
[8] G. Kreiss, A. Lundbladh, and D. S. Henningson, "Bounds for threshold amplitudes in subcritical shear flows," J. Fluid Mech. **270**, 175 (1994).
[9] A. Lundbladh, D. S. Henningson, and S. C. Reddy, "Threshold amplitudes for transition in channel flow," to appear in the *Proceedings of the ICASE Workshop on Transition, Turbulence and Combustion*, 1993.